Prediction of Material Behavior of Ceramic Matrix Composites under Static Tensile Loading

HARUYAMA Daichi : Doctor of Engineering, Material and Structural Engineering Department, Technology Platform Center, Corporate Research and Development Division, IHI Corporation

Improving aircraft fuel efficiency requires the application of high-temperature and high-strength ceramic matrix composites (CMCs) to engine components, necessitating enhanced material properties, highly accurate structural strength predictions, and a thorough understanding of fracture mechanisms. In this study, damage models under static tensile loading in the fiber direction of unidirectional CMCs were constructed to enable precise prediction of the material behavior of unidirectional CMCs. By employing both matrix crack growth and fiber breakage models, it is possible to accurately predict the stress–strain and crack density–stress relationships obtained in experiments.

1. Introduction

In recent years, in the aircraft industry, the demand for reducing environmental impact to realize a sustainable society has been increasing. As one of the efforts to reduce environmental impact, technological development aimed at improving fuel efficiency has been carried out. Methods for improving fuel efficiency include increasing the turbine inlet temperature and reducing aircraft weight. One technology that can contribute to these methods is the application of ceramic matrix composites (CMCs) to engine components. To date, research and development aimed at applying CMCs to various engine components has progressed, and the development of high-strength CMCs applicable in higher temperature environments is required for further improvements in fuel efficiency. To achieve this, it is necessary to improve material properties and accurately predict strength. To improve material properties, in addition to enhancing the properties of individual materials, appropriate combinations of constituent materials are important, and accurate strength prediction requires a sufficient understanding of fracture phenomena. Therefore, it is important to accurately predict the behavior of composites by modeling the fracture phenomena of constituent materials such as fibers, interphases, and matrices. **Figure 1** shows the microscopic damage in unidirectional CMCs. When a load is applied in the fiber direction of unidirectional CMCs, matrix cracks form. However, to prevent brittle fracture of the entire CMCs, the material is designed so that the matrix cracks do not propagate into the fibers, but instead are deflected toward the fiber/matrix interfaces, resulting in interfacial debonding. As the load is further increased, matrix cracks form at multiple locations, and interfacial debonded regions between the fibers and matrix expand, eventually suppressing the formation of additional matrix cracks. Furthermore, fibers fracture locally at mechanically weak regions and eventually break when the fibers can no longer withstand the applied load. The mechanical properties change as these types of microscopic damage develop.

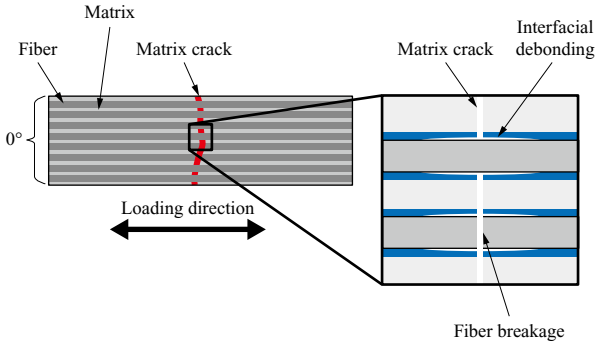


Fig. 1 Schematic of damages in unidirectional CMCs

Therefore, this study aimed to establish a damage model for unidirectional CMCs under static tensile loading in the fiber direction and to accurately predict the material behavior of unidirectional CMCs, including the stress–strain relationship and crack growth process. Calculations were performed using the developed damage model, and the validity of the model was verified by comparing the calculated results with the experimental results.

2. Random matrix crack growth model

2.1 Energy release rate associated with matrix crack formation

This section presents the energy release rate associated with matrix crack formation, which is necessary for simulating matrix crack growth. **Figure 2** shows a new matrix crack formed between existing matrix cracks. The energy release rate $d\overline{\xi}_m$ associated with a new matrix crack formation is given by Equations (2-1) to (2-6)[1].

$$d\overline{\xi}_m^I = \overline{\xi}_0 + 3\overline{\xi}_0 \frac{\sigma_{deb}}{\sigma_1 + \sigma_{th} - \sigma_{deb}} \quad \cdots\cdots\cdots\cdots\cdots\cdots \text{(2-1)}$$

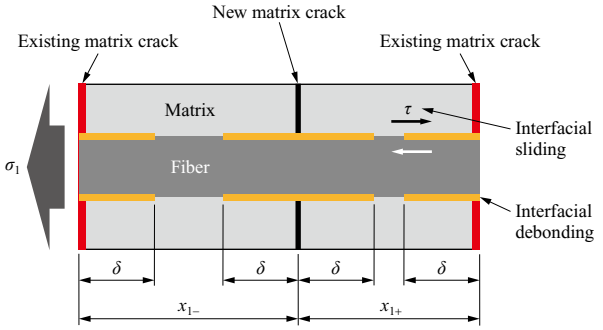


Fig. 2 New matrix crack initiation between pre-existing matrix cracks

$$d\bar{\xi}_m^{II} = \bar{\xi}_0\left[1-2\left(1-\frac{x_{1+}}{2\delta}\right)^3\right] + 3\bar{\xi}_0\frac{\sigma_{deb}}{\sigma_1+\sigma_{th}-\sigma_{deb}}\left[-2\left(\frac{x_{1+}}{2\delta}\right)^2+4\left(\frac{x_{1+}}{2\delta}\right)-1\right] \quad \cdots\cdots (2\text{-}2)$$

$$d\bar{\xi}_m^{III} = \bar{\xi}_0\left[-6\left(\frac{x_{1+}}{2\delta}\right)^3+6\left(\frac{x_{1+}}{2\delta}\right)^2\right] + 3\bar{\xi}_0\frac{\sigma_{deb}}{\sigma_1+\sigma_{th}-\sigma_{deb}}\left[2\left(\frac{x_{1+}}{2\delta}\right)^2\right] \quad \cdots\cdots (2\text{-}3)$$

$$d\bar{\xi}_m^{IV} = \bar{\xi}_0\left[1-2\left\{\left(1-\frac{x_{1+}}{2\delta}\right)^3+\left(1-\frac{x_{1-}}{2\delta}\right)^3\right\}\right] + 3\bar{\xi}_0\frac{\sigma_{deb}}{\sigma_1+\sigma_{th}-\sigma_{deb}}\left[-2\frac{x_{1+}^2+x_{1-}^2}{(2\delta)^2}+4\frac{x_{1+}+x_{1-}}{2\delta}-3\right] \quad \cdots\cdots (2\text{-}4)$$

$$d\bar{\xi}_m^{V} = \bar{\xi}_0\left[-6\left(\frac{x_{1+}}{2\delta}\right)^3+6\left(\frac{x_{1+}}{2\delta}\right)^2+2\left(\frac{x_{1-}}{2\delta}\right)^3-6\left(\frac{x_{1-}}{2\delta}\right)^2+6\frac{x_{1-}}{2\delta}-2\right] + 3\bar{\xi}_0\frac{\sigma_{deb}}{\sigma_1+\sigma_{th}-\sigma_{deb}}\left[2\left(\frac{x_{1+}}{2\delta}\right)^2-2\left(\frac{x_{1-}}{2\delta}\right)^2+4\frac{x_{1-}}{2\delta}-2\right] \quad \cdots\cdots (2\text{-}5)$$

$$d\bar{\xi}_m^{VI} = \bar{\xi}_0\left[-2\left(\frac{x_{1+}}{2\delta}\right)^3+6\left(\frac{x_{1-}}{2\delta}\right)\left(\frac{x_{1+}}{2\delta}\right)^2\right] \quad \cdots\cdots (2\text{-}6)$$

$$\bar{\xi}_0 = \frac{(\sigma_1+\sigma_{th}-\sigma_{deb})^3 V_m^2 E_m^2 r_f}{6V_f^2 E_f \tau E_1^2} \quad \cdots\cdots (2\text{-}7)$$

$$\delta = \frac{V_m E_m}{V_f E_1}\frac{r_f}{2\tau}(\sigma_1+\sigma_{th}-\sigma_{deb}) \quad \cdots\cdots (2\text{-}8)$$

$$\sigma_{th} = V_f E_f(\alpha_f-\alpha_m)(T-T_0) = V_f E_f(\alpha_f-\alpha_m)\Delta T \quad \cdots\cdots (2\text{-}9)$$

$$\sigma_{deb} = 2V_f\sqrt{\frac{E_f E_1 \Gamma_d}{V_m E_m r_f}} \quad \cdots\cdots (2\text{-}10)$$

where $\bar{\xi}_0$ is the reference energy release rate, σ_1 is the tensile stress, σ_{th} is the thermal residual stress, σ_{deb} is the interfacial debonding stress, x_{1+} and x_{1-} are the distances to adjacent cracks, δ is the interfacial debonding length, r_f is the fiber radius, τ is the interfacial frictional stress, V_f is the fiber volume fraction of the unidirectional composite, V_m is the matrix volume fraction of the unidirectional composite, E_f is the longitudinal elastic modulus of the fiber, E_m is the longitudinal elastic modulus of the matrix, E_1 is the longitudinal elastic modulus in the fiber direction of the unidirectional composite, α_f is the thermal expansion coefficient of the fiber, α_m is the thermal expansion coefficient of the matrix, T is the temperature, T_0 is the temperature at which the thermal residual stress is zero, and Γ_d is the critical energy release rate for interfacial debonding. Superscripts *I* to *VI* indicate the classifications according to the relative positions of the matrix cracks and the overlap conditions of the interfacial debonding regions[2]. Cases *I* to *V* correspond to equations obtained by adding a second term representing the effects of the thermal residual stress σ_{th} and interfacial debonding stress σ_{deb} to the equations of Zok and Spearing[2], whereas Case *VI* corresponds to the equations of Zok and Spearing.

2.2 Calculation of matrix crack growth using the Monte Carlo method

Using the matrix crack growth model formulated in **Section 2.1** in combination with the Monte Carlo method, a calculation model considering the variation of defects was developed under the assumption that matrix cracks are formed by the local fracture energy (critical energy release rate) within the matrix, and the stress–strain relationship and crack density were calculated. **Figure 3** shows the calculation model. A calculation region having a length L in the fiber direction was considered, and the formed cracks were assumed to penetrate the calculation region. The calculation region was divided into N elements in the fiber direction, and the size of each element at its location was defined as $\Delta l = L/N$. In addition, at position i, the distances to the adjacent cracks were defined as x_{1+} and x_{1-}, and the energy

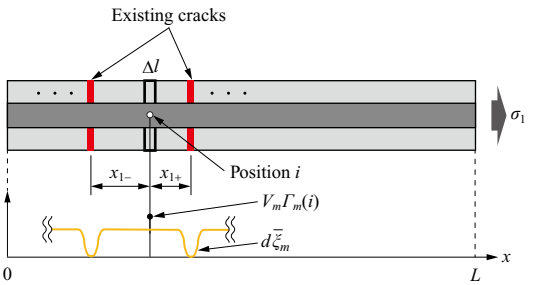


Fig. 3 Computational model

release rate $d\bar{\xi}_m$ due to matrix crack formation was calculated using Equations (2-1) to (2-6), depending on the relative positions of the interfacial debonding length δ and the cracks. Equations (2-2) to (2-6) were derived under the condition $x_{1+} \le x_{1-}$; in the case of $x_{1+} > x_{1-}$, x_{1+} and x_{1-} should simply be interchanged. Moreover, matrix cracks were assumed to be formed when Equation (2-11) is satisfied.

$$d\bar{\xi}_m \ge V_m \Gamma_m(i) \quad \cdots\cdots (2\text{-}11)$$

where $\Gamma_m(i)$ is the fracture energy of the matrix at position i, which is assumed to depend on the defect distribution. The variation in the matrix fracture energy was assumed to follow a Weibull distribution. Specifically, using the Weibull distribution R_i given by Equation (2-12), random numbers following the Weibull distribution were generated from uniformly distributed random numbers by the inverse transform method, and the fracture energy $\Gamma_m(i)$ at each position was then calculated.

$$R_i = 1 - \exp\left(-\frac{\Delta V}{V_{m0}}\left(\frac{\Gamma_m(i)}{\Gamma_{ms}}\right)^{\Gamma_{mg}}\right) \quad \cdots\cdots (2\text{-}12)$$

where Γ_{ms} is the scale parameter, Γ_{mg} is the shape parameter, V_{m0} is the reference volume, and ΔV is the volume of each divided element. The volume was defined as the volume per unit width obtained by dividing by the width of the test specimen, and the reference volume V_{m0} was assumed to follow Equation (2-13).

$$V_{m0} = L \times b_r \times V_m \quad \cdots\cdots (2\text{-}13)$$

where b_r is the reference thickness. In addition, the volume ΔV of each divided element is given by Equation (2-14).

$$\Delta V = \Delta l \times b_r \times V_m \quad \cdots\cdots (2\text{-}14)$$

Moreover, the crack density ρ_1 was calculated from the number of cracks n and the length L, as given by Equation (2-15).

$$\rho_1 = \frac{n}{L} \quad \cdots\cdots (2\text{-}15)$$

Furthermore, the average strain ϵ_1 over the entire calculation region was defined as the average of the fiber strain $\epsilon_f^m(i)$ at each position i.

$$\epsilon_1 = \frac{1}{L}\sum_{n=1}^{N}\epsilon_f^m(i)\Delta l \quad \cdots\cdots (2\text{-}16)$$

The fiber strain $\epsilon_f^m(i)$ at each position i was calculated using Equations (2-17) to (2-20)[1], taking into consideration the distances to the adjacent cracks x_{1+} and x_{1-}.

$$\epsilon_f^m(i) = \epsilon_1^0 \quad \text{for } x_{1+} \ge \delta \text{ and } x_{1-} \ge \delta \quad \cdots\cdots (2\text{-}17)$$

$$\epsilon_f^m(i) = (1+\beta)\epsilon_1^0 - \beta\left(\epsilon_1^m + \epsilon_{th} - \epsilon_{deb}\right)\frac{x_{1-}}{\delta} + \beta\epsilon_{th}$$
$$\text{for } x_{1-} \le x_{1+} \text{ and } x_{1-} < \delta \quad \cdots\cdots (2\text{-}18)$$

$$\epsilon_f^m(i) = (1+\beta)\epsilon_1^0 - \beta\left(\epsilon_1^m + \epsilon_{th} - \epsilon_{deb}\right)\frac{x_{1+}}{\delta} + \beta\epsilon_{th}$$
$$\text{for } x_{1-} \ge x_{1+} \text{ and } x_{1+} < \delta \quad \cdots\cdots (2\text{-}19)$$

$$\beta = \frac{V_m E_m}{V_f E_f} \quad \cdots\cdots (2\text{-}20)$$

where ϵ_1^0 is the strain of the unidirectional composite without damage, ϵ_{th} is the thermal strain, ϵ_{deb} is the strain associated with the interfacial debonding, as given by Equations (2-21) to (2-23).

$$\epsilon_1^0 = \frac{\sigma_1}{E_1} \quad \cdots\cdots (2\text{-}21)$$

$$\epsilon_{th} = \frac{\sigma_{th}}{E_1} \quad \cdots\cdots (2\text{-}22)$$

$$\epsilon_{deb} = \frac{\sigma_{deb}}{E_1} \quad \cdots\cdots (2\text{-}23)$$

In addition, β is a material constant related to the fiber and matrix.

2.3 Parameters used in the calculations

To validate the calculation model, the experimental results[3), (4)] for a unidirectional CMC laminate $[0]_{12}$ composed of silicon carbide (SiC) fibers and a calcium alumino-silicate (CAS) matrix were used. In the calculation model, L = 10 mm, N = 10,000, and the maximum stress σ_{1max} = 400 MPa were used. The material parameters are listed in **Table 1**. The reference thickness b_r was defined as the thickness of the test specimen. Moreover, this calculation model requires the values of material parameters such as the parameters Γ_{ms} and Γ_{mg} related to the fracture energy of the matrix, the interfacial debonding energy Γ_d, and the interfacial shear stress τ. Specific values of the interfacial debonding energy and the interfacial shear stress are listed in **Table 2**. Although various measurement methods have been proposed, the measured values differ significantly depending on the methods. Therefore, to determine the values of the parameters, the ranges were narrowed by varying the value of the interfacial debonding energy Γ_d and calculating the interfacial shear stress τ and the parameters Γ_{ms} and Γ_{mg} related to the fracture energy of the matrix when the calculated stress–strain

Table 1 Parameters of unidirectional SiC/CAS composites

Symbol	Explanation	Value	Unit
E_f	Young's modulus of the fiber	190[3), (4)]	GPa
α_f	Thermal expansion coefficient of the fiber	3.3×10^{-6}[3), (4)]	K^{-1}
E_m	Young's modulus of the matrix	90[3), (4)]	GPa
α_m	Thermal expansion coefficient of the matrix	4.6×10^{-6}[3), (4)]	K^{-1}
V_f	Fiber volume fraction	0.34[3), (4)]	—
ΔT	Temperature difference during forming	−1,200[3)]	K
r_f	Fiber radius	8[3)]	μm
b_r	Reference thickness	2.1[3)]	mm

Table 2 Interface sliding stress and interface debonding energy of SiC/CAS by each method

Explanation	Method	Value	Unit
Interfacial shear stress τ	Matrix crack stress	10 to 15[9)]	MPa
	Fiber bundle push-out	14 to 19[5)]	MPa
	Push-down using the Marshall model	29±3 (load)[10), (11)] 21±2 (maximum load)	MPa
Interfacial debonding energy Γ_d	Fiber bundle push-out	≈ 0.0[5), (6)]	J/m^2
	Non-elastic strain	0.1[7)]	J/m^2
	Permanent strain	0.3[12)]	J/m^2
	Hysteresis analysis	0.5±0.3[6), (8)]	J/m^2

relationship and crack density–stress relationship agreed with the experimental results. Regarding the minimum value of the interfacial debonding energy, fiber bundle push-out tests indicated a value of approximately 0.0 J/m^2[5), (6)]; however, no explicit value was presented. In contrast, He et al. used 0.1 J/m^2[7)] as the interfacial debonding energy in their study of inelastic strain. Since it is difficult to consider the interfacial debonding energy to be 0.0 J/m^2, a value of 0.1 J/m^2 was also used in this study. In addition, for the interfacial debonding energy, the value obtained by the hysteresis analysis method, which showed the maximum value among the investigated results, namely 0.8 J/m^2[6), (8)], was also used in the calculations.

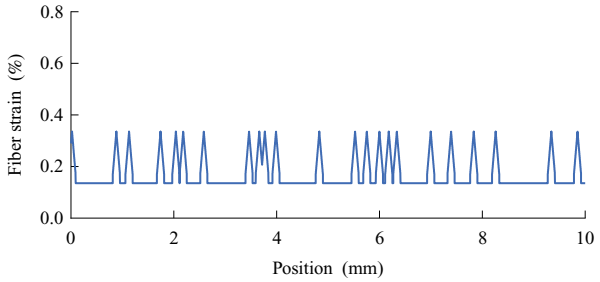
2.4 Calculation results

Table 3 lists the parameters adjusted so that the calculated results agree well with the stress–strain and crack density–stress relationships obtained in the experiment[3)]. First, a Monte Carlo simulation was performed to confirm whether random matrix crack growth could be simulated. **Figure 4** shows the distribution of the axial fiber strain ϵ_f^m as a solid blue line, the matrix energy release rate $d\bar{\xi}_m$ as a solid orange line, and the fracture energy distribution $V_m\Gamma_m$ as black dots. It was confirmed that cracks were formed when the matrix energy release rate exceeded the fracture energy at a certain position, resulting in a reduction in the matrix energy release rate and the development of a strain distribution in the fibers. It was also confirmed that random crack growth occurred through repeated redistribution of the matrix energy release rate and fiber strain due to crack formation, together with the increase in stress.

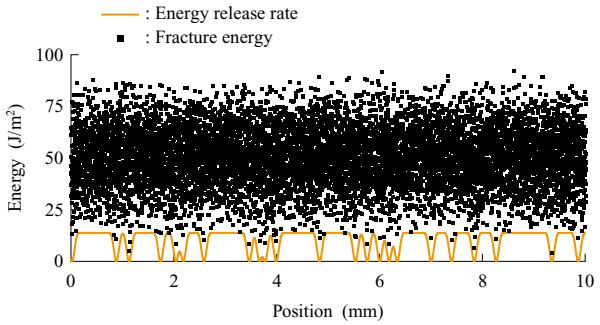
Next, the stress–strain and crack density–stress relationships obtained from three Monte Carlo simulations are shown in **Figs. 5** and **6**, respectively. Almost no variation was observed in the stress–strain relationships, whereas the crack density–stress showed variations comparable to those in the experimental results. Therefore, it was found that variations

Table 3 Parameter adjustment results for each case

Case	Γ_d (J/m^2)	τ (MPa)	Γ_{ms} (J/m^2)	Γ_{mg} (–)
1	0.1	18	15	4
2	0.8	13	10	3

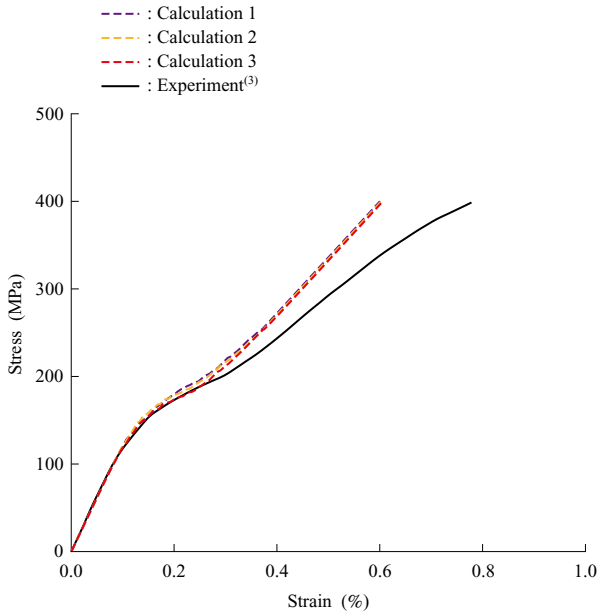


(a) Fiber strain

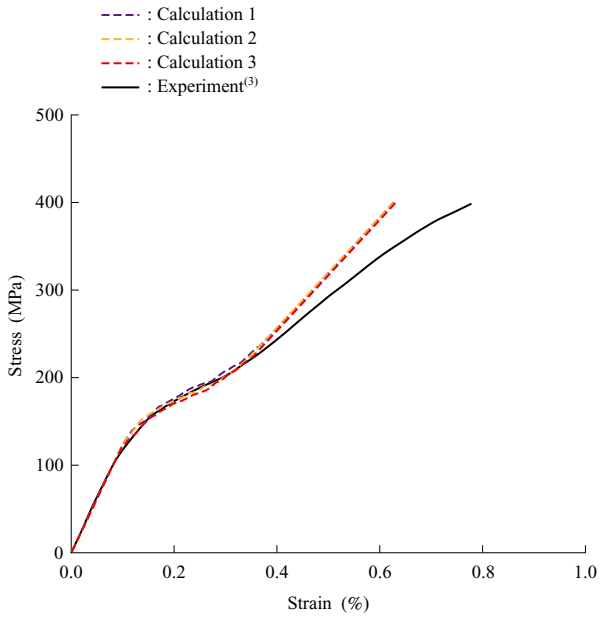


(b) Energy release rate and fracture energy

Fig. 4 Distribution of fiber strain, energy release rate of matrix, and fracture energy

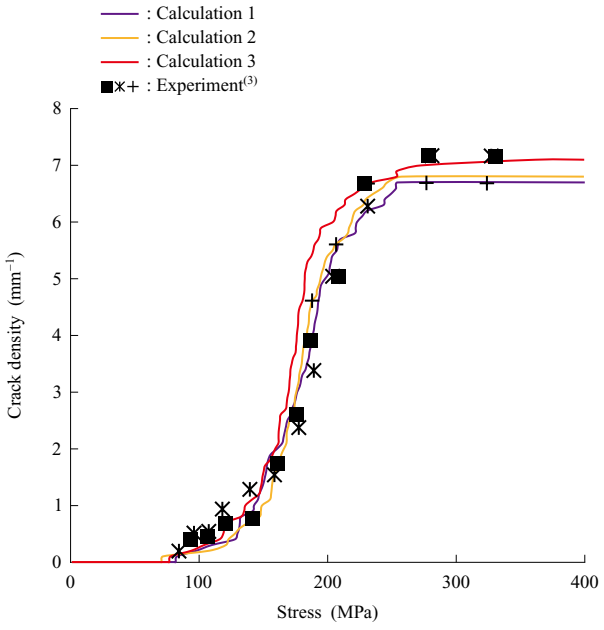


(a) Case 1

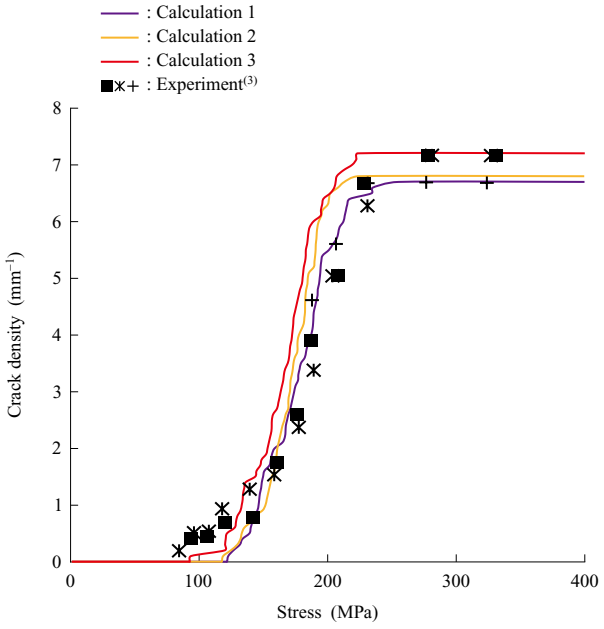


(b) Case 2

Fig. 5 Stress–strain curves obtained by calculation and experiment



(a) Case 1



(b) Case 2

Fig. 6 Crack density–stress relationships obtained by calculation and experiment

in fracture energy have no significant effect on the parameters. Furthermore, for Cases 1 and 2, the calculated and experimental stress–strain relationships showed good agreement up to the initial pseudo-ductile region, while the calculated and experimental crack density–stress relationships showed good agreement throughout the entire process from crack initiation to saturation. However, after crack saturation, the stress–strain relationships no longer agreed. Assuming that the matrix does not bear the load and that the fibers remain intact, $V_f E_f$ was calculated as 64.6 GPa, which differs from the experimental tangent modulus of approximately 45 GPa. This discrepancy is considered to be due to the neglect of fiber breakage. Fiber breakage will be discussed in **Chapter 4**.

In addition, although the present calculations narrowed the ranges of the interfacial debonding energy Γ_d, interfacial shear stress τ, scale parameter Γ_{ms}, and shape parameter Γ_{mg}, it is necessary to determine the value of each parameter for further calculations. Here, the details of the stress–strain relationships in **Fig. 5** and the crack density–stress relationships in **Fig. 6** were reexamined. Near the stress of 200 MPa, where matrix crack growth was observed, the calculated results reflected stress reduction caused by fiber breakage associated with matrix cracking. Therefore, the calculated and experimental results near a stress of 150 MPa, where matrix cracks began to initiate and the influence of fiber breakage was negligible, were examined. In the stress–strain relationships shown in **Fig. 5**, no clear difference was observed between Cases 1 and 2, whereas in the crack density–stress relationships shown in **Fig. 6**, Case 1 showed better agreement between the calculated and experimental results than Case 2. In Case 2, the calculated and experimental results for the matrix crack initiation stress could not be matched by parameter adjustment, and the calculated results were higher than the experimental results. This is considered to be due to the large interfacial debonding energy. When matrix cracking and interfacial debonding occur, the energy supplied by the applied load is consumed by the interfacial debonding, thereby reducing the energy available for matrix crack initiation. This is considered to be the reason why the calculated matrix crack initiation stress becomes higher. Based on the above discussion, the parameters of Case 1 were used in the subsequent calculations.

3. Periodic matrix crack growth model

3.1 Calculation model

In **Chapter 2**, the random matrix crack growth model made it possible to represent the stress–strain relationships and crack density–stress relationships up to a stress of approximately 200 MPa, at which matrix cracking saturates. However, to understand fracture phenomena over a wide region, such as those occurring in textile composites and components, it is necessary from the viewpoint of computational cost to use a model that replaces random material behavior, including local effects, with averaged material behavior. Thus, a periodic matrix crack growth model considering variations in defects was formulated, and it was examined whether calculation results equivalent to the stress–strain relationships and crack density–stress relationships obtained from the Monte Carlo simulations could be reproduced.

First, in the periodic matrix crack growth model shown in **Fig. 2**, it was assumed that a new crack forms at the midpoint between adjacent cracks. In this case, the energy release rate $d\bar{\xi}_m$ due to matrix cracking varies depending on the interfacial debonding length δ and the crack spacing $\bar{x}_1$ and is given by Equations (2-1), (2-4), and (2-6) in **Section 2.1** with $x_{1+} = x_{1-} = \bar{x}_1$. Here, since crack formation is assumed to occur periodically, the average crack spacing $\bar{x}_1$ differs from the results obtained from the Monte Carlo simulations. Therefore,

a correction coefficient was applied to the average crack spacing $\bar{x}_1$ and the modified average crack spacing $\bar{x}_1^*$, which takes variation in crack positions into account, was introduced.

$$d\bar{\xi}_m = \bar{\xi}_0 + 3\bar{\xi}_0 \frac{\sigma_{deb}}{\sigma_1 + \sigma_{th} - \sigma_{deb}} \quad \text{for } 2 < \bar{x}_1^* / \delta \quad \cdots\cdots (3\text{-}1)$$

$$d\bar{\xi}_m = \bar{\xi}_0 \left[1 - 4\left(1 - \frac{\bar{x}_1^*}{2\delta}\right)^3 \right] + 3\bar{\xi}_0 \frac{\sigma_{deb}}{\sigma_1 + \sigma_{th} - \sigma_{deb}} \left[-4\left(\frac{\bar{x}_1^*}{2\delta}\right)^2 + 8\left(\frac{\bar{x}_1^*}{2\delta}\right) - 3 \right]$$

$$\text{for } 1 \le \bar{x}_1^* / \delta \le 2 \quad \cdots\cdots (3\text{-}2)$$

$$d\bar{\xi}_m = \bar{\xi}_0 \times 4\left(\frac{\bar{x}_1^*}{2\delta}\right)^3 \quad \text{for } 0 \le \bar{x}_1^* / \delta \le 1 \quad \cdots\cdots (3\text{-}3)$$

$$\bar{x}_1^* = \Lambda \bar{x}_1 \quad \cdots\cdots (3\text{-}4)$$

The correction coefficient Λ was set to 1.337, as obtained from a theoretical one-dimensional random packing problem[13), (14)].

Next, Equation (3-5) was used as the condition for crack growth.

$$d\bar{\xi}_m \ge V_m \Gamma_{mR} \quad \cdots\cdots (3\text{-}5)$$

where Γ_{mR} is the fracture energy of the matrix. The relationship between the fracture energy and crack density obtained from the Monte Carlo simulations, together with the fitting curve, is shown in **Fig. 7**. Since the fracture energy increases during the crack growth process, the matrix fracture energy Γ_{mR} was assumed to satisfy Equation (3-6) as a function of crack density $\bar{\rho}_1^*$ considering variations.

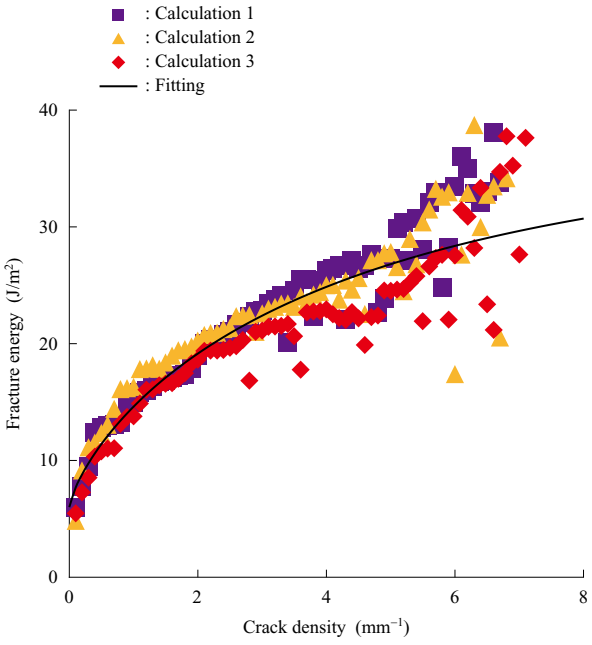


Fig. 7 Fitting curve for fracture energy vs. crack density calculated by Monte Carlo method

$$\Gamma_{mR}(\bar{\rho}_1^*) = \Gamma_{m0} + (\Gamma_{m_{max}} - \Gamma_{m0}) \left(1 - \exp\left(-\left(\frac{\bar{\rho}_1^*}{\rho_0}\right)^a\right)\right) \quad \cdots\cdots (3\text{-}6)$$

where Γ_{m0} is the initial fracture energy, $\Gamma_{m_{max}}$ is the maximum fracture energy, ρ_0 is the characteristic crack density, and a is the coefficient related to defect variations. Using the crack density–fracture energy relationship obtained from three Monte Carlo simulations for Case 1 in **Table 3**, each parameter was determined by the least-squares method under the constraint condition of $\Gamma_{m0} = 6$ J/m^2[3)]. The parameters for the fitting curve are $\Gamma_{m_{max}} = 37.1$ J/m^2, $\rho_0 = 4.38$ mm^{-1}, and $a = 0.763$. Furthermore, for each stress σ_1, the crack density $\bar{\rho}_1^*$, which takes into account the variations when the equality in Equation (3-5) is satisfied, was numerically calculated. In this calculation, assuming that the crack density is periodic, the relationship between crack spacing and crack density expressed by Equation (3-7) was used.

$$\bar{\rho}_1^* = \frac{1}{\bar{x}_1^*} \quad \cdots\cdots (3\text{-}7)$$

Next, the relationship between stress and strain was obtained. When the midpoint between newly formed cracks is taken as the origin, the average strain of the entire composite, ϵ_1, is given by Equation (3-8), where the fiber strain is averaged over the crack spacing because the cracks are periodically aligned.

$$\epsilon_1 = \frac{2}{\bar{x}_1^*} \int_0^{\bar{x}_1^*/2} \epsilon_f^m dx \quad \cdots\cdots (3\text{-}8)$$

The calculation results are given in Equations (3-9) and (3-10)[1)].

$$\epsilon_1 = \frac{\sigma_1}{E_1} + \frac{V_m E_m}{V_f E_f E_1} \frac{\delta}{\bar{x}_1^*} (\sigma_1 + \sigma_{th} + \sigma_{deb})$$

$$\text{for } 1 \le \bar{x}_1^* / 2\delta \quad \cdots\cdots (3\text{-}9)$$

$$\epsilon_1 = \frac{\sigma_1}{V_f E_f} + \frac{V_m E_m}{V_f E_f E_1} \sigma_{th} - \frac{V_m E_m}{V_f E_f E_1} \frac{\bar{x}_1^*}{4\delta} (\sigma_1 + \sigma_{th} - \sigma_{deb})$$

$$\text{for } 1 \ge \bar{x}_1^* / 2\delta \quad \cdots\cdots (3\text{-}10)$$

3.2 Calculation results

The calculation results for random matrix crack growth obtained by the Monte Carlo simulations were compared with those for the periodic matrix crack growth model that takes defect variations into consideration. **Figure 8** shows the stress–strain relationship and **Fig. 9** shows the crack density–stress relationship. Λ = 1 represents the case in which the effect of variations in matrix cracks is not taken into consideration, whereas Λ = 1.337 represents the case in which the effect of variations in matrix cracks is taken into consideration. By applying the correction coefficient Λ = 1.337, the calculation results for random matrix crack growth agreed well with those for periodic matrix crack growth.

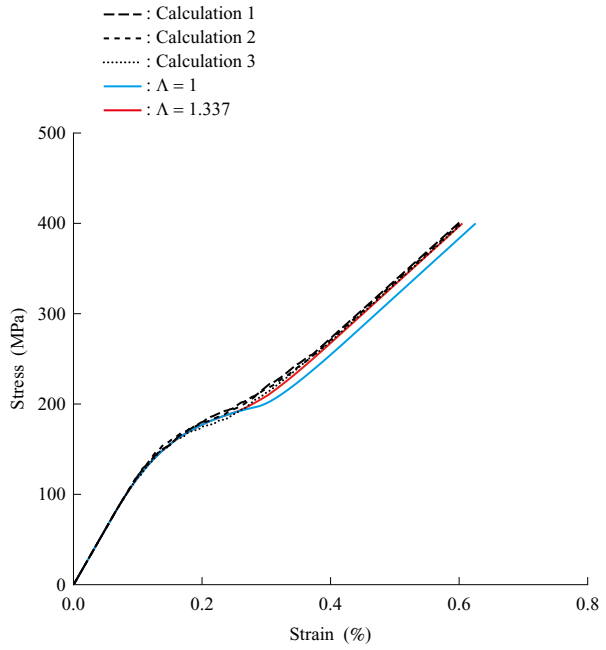


Fig. 8 Stress–strain curves calculated by Monte Carlo method and periodic matrix crack growth model

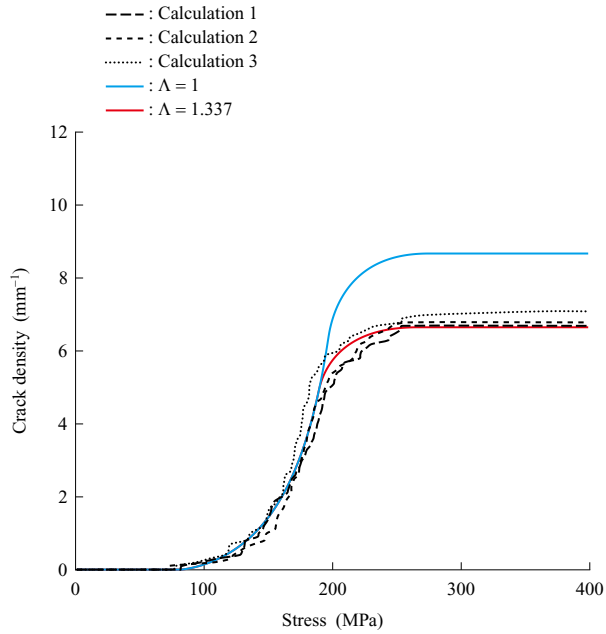


Fig. 9 Crack density–stress curves calculated by Monte Carlo method and periodic matrix crack growth model

4. Fiber breakage model

4.1 Calculation model

Since the strength of brittle materials such as ceramic fibers is determined by the size, shape, and distribution of microscopic defects in the material, the strength of individual fibers exhibits probabilistic variations. Therefore, a probabilistic fiber breakage model based on the Weibull distribution was applied. The fiber breakage probability, P_f, is given by Equation (4-1)[1), (15)].

$$P_f(x_0, S) = 1 - \exp\left\{-\frac{1}{m_f+1}\left(\frac{S}{\sigma_c}\right)^{m_f+1}\left[1-\left(1-\frac{x_0}{l_s}\right)^{m_f+1}\right]\right\} \quad \cdots\cdots (4\text{-}1)$$

where S is the fiber stress, l_s is the recovery length of fiber stress, σ_c is the characteristic stress, m_f is the Weibull shape factor, and x_0 is the range of fiber stress variation caused by fiber breakage. In addition, when determining the strength of composites, it is important to estimate how the load carried by broken fibers is redistributed to the unbroken fibers. Therefore, the global load sharing (GLS) model, in which the load carried by a fractured fiber is equally redistributed among all the remaining fibers after fiber breakage, was adopted. The GLS model is given by Equations (4-2) to (4-4)[15].

$$\frac{\sigma_1}{V_f} = [1-F_R]S + F_R\frac{S}{2} \quad \cdots\cdots (4\text{-}2)$$

$$F_R = P_{d_{ini}} + \left(P_p + (1-P_{d_{ini}})(1-P_p)P_f\right)\frac{2l_s}{\bar{x}_1^*} \quad \cdots\cdots (4\text{-}3)$$

$$P_{d_{ini}} = 1 - \exp\left(-\frac{2l_s f_d}{\delta_c}\right) \quad \cdots\cdots (4\text{-}4)$$

where F_R is the fiber breakage probability within the range $2l_s$, $P_{d_{ini}}$ is the fiber breakage probability due to initial damage, P_p is the probability that a matrix crack propagates into a fiber, δ_c is the characteristic length, and f_d is the number of defects for initial damage per δ_c. **Figure 10** shows matrix cracks and fiber breakage in the GLS model. Fiber damage was classified into initial damage, fiber breakage associated with matrix cracks, and fiber breakage due to applied loading. The fiber stress S is obtained by numerically solving the nonlinear Equation (4-2). When the balance between the fiber stress and the tensile stress can no longer

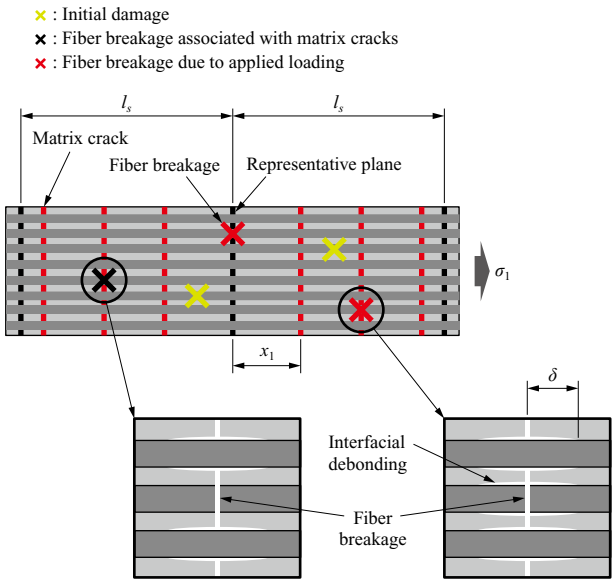


Fig. 10 Matrix crack and fiber breakage in GLS model

be maintained, that is, when σ_1 attains its maximum value, the composite reaches its ultimate fracture strength.

Furthermore, since the GLS model tends to overestimate strain, calculations based on the local load sharing (LLS) model, which takes the effects of local fiber breakage into consideration, were also performed. The LLS model adopted in this study was based on a method that can utilize the fracture strength obtained from the GLS model. The probability $H_{n_f L_z}$ of a fiber bundle is given by Equations (4-5) and (4-6)[15].

$$H_{n_f L_z}(\sigma_{fb}) = 1 - \left(1 - \Phi\left(\left(\sigma_{fb} - \mu^*_{n_l}\right) / \gamma^{**}_{n_l}\right)\right)^{n'} \quad \cdots (4\text{-}5)$$

$$\mu^*_{n_l} = \mu + \Delta_{n_l} \quad \cdots (4\text{-}6)$$

where σ_{fb} is the fiber bundle stress, Φ is the cumulative distribution function of a Gaussian distribution with mean $\mu^*_{n_l}$ and standard deviation $\gamma^{**}_{n_l}$ both taking account of local effects in the fiber bundle strength, n' is a ratio of the minimum region determining the ultimate fracture within the evaluation region, μ is the ultimate fracture strength of the composite obtained from the GLS model, and Δ_{n_l} is the strength correction for the critical number of fibers n_l[16),(17)]. Using these equations, the fracture strength σ^*_{fb} at $H_{n_f L_z}(\sigma^*_{fb}) = 0.5$ was obtained.

Finally, the strain increment $\Delta\epsilon$ due to fiber breakage is given by Equations (4-7) and (4-8).

$$\Delta\epsilon = \frac{1}{E_f}\left(S - \frac{\sigma_1}{V_f}\right)\left(\frac{2\delta}{\bar{x}^*_1}\right) \quad \text{for } 1 \le \bar{x}^*_1 / 2\delta \quad \cdots (4\text{-}7)$$

$$\Delta\epsilon = \frac{1}{E_f}\left(S - \frac{\sigma_1}{V_f}\right) \quad \text{for } 1 \ge \bar{x}^*_1 / 2\delta \quad \cdots (4\text{-}8)$$

This strain increment is added to the strain given by Equations (3-9) and (3-10) presented in **Section 3.1**. Accordingly, the relationship between stress and strain is given by Equations (4-9) and (4-10).

$$\epsilon_1 = \frac{\sigma_1}{E_1} + \frac{V_m E_m}{V_f E_f E_1}\frac{\delta}{\bar{x}^*_1}\left(\sigma_1 + \sigma_{th} + \sigma_{deb}\right) + \Delta\epsilon \quad \text{for } 1 \le \bar{x}^*_1 / 2\delta \quad \cdots (4\text{-}9)$$

$$\epsilon_1 = \frac{\sigma_1}{V_f E_f} + \frac{V_m E_m}{V_f E_f E_1}\sigma_{th} - \frac{V_m E_m}{V_f E_f E_1}\frac{\bar{x}^*_1}{4\delta}\left(\sigma_1 + \sigma_{th} - \sigma_{deb}\right) + \Delta\epsilon \quad \text{for } 1 \ge \bar{x}^*_1 / 2\delta \quad \cdots (4\text{-}10)$$

4.2 Parameters used in the calculations

The parameters used in the calculations are listed in **Tables 1** and **4**. The material parameters for fiber breakage were obtained from fracture mirror observations in tensile tests of the SiC/CAS composites and used in the calculations[18]. Since this strength includes the effect of initial damage, the number of initial defects, f_d, was set to 0. In addition, the method proposed by Haruyama et al.[1] was adopted to determine the probability P_p of crack propagation from the matrix to the fiber. Specifically, the probability was determined from the relationship between the elastic modulus ratio and the energy release rate ratio with the conditions of crack propagation into dissimilar materials and crack deflection along the interface, as proposed by He et al.[19], together with the Weibull cumulative probability plot of the interfacial debonding stress obtained from the push-out test. Since the Weibull cumulative probability plot data for the interfacial debonding stress of SiC/CAS composites could not be found in the literature, the results for SiC/SiC composites consisting of Nicalon® fibers and a SiC matrix fabricated by the chemical vapor infiltration (CVI) process were used instead[20]. First, according to the results of He et al., the condition for matrix crack propagation into the fibers is given as follows, where Γ_f is the fracture energy of the fibers.

$$\frac{\Gamma_d}{\Gamma_f} = 0.385 \quad \cdots (4\text{-}11)$$

Moreover, using the fracture toughness of SiC (Nicalon) fibers, $K_f \approx 1$ MPa·m$^{1/2}$[21], the fracture energy was obtained as follows.

$$\Gamma_f = \frac{K_f^2}{E_f} = 5.26\ \left(\mathrm{J/m^2}\right) \quad \cdots (4\text{-}12)$$

Furthermore, from Equations (2-10), (4-11) and (4-12), the interfacial debonding when the matrix cracks propagate into the fibers was obtained as $\sigma^*_{deb} = 215.6$ MPa. This value was substituted into the Weibull cumulative probability plot of the interfacial debonding stress given by Equation (4-13).

$$F\left(\sigma^*_{deb}\right) = 1 - \exp\left\{-\left(\frac{\sigma^*_{deb} - \gamma}{\sigma_{d_0}}\right)^{m_d}\right\} \quad \cdots (4\text{-}13)$$

Using the parameters of $\gamma = 0$ MPa, $m_d = 1.0081$, and $\sigma_{d_0} = 61.793$ MPa[1], $F\left(\sigma^*_{deb}\right) = 0.94$ was obtained. When the interfacial debonding stress is high, matrix cracks propagate into the fibers without being deflected at the interface. Therefore, assuming that matrix cracks propagate into the fibers when the interfacial debonding stress exceeds a certain value σ^*_{deb}, the cumulative probability $1 - F\left(\sigma^*_{deb}\right)$ can be

Table 4 Parameters of unidirectional SiC/CAS composites on matrix cracks and fiber breakage

Symbol	Explanation	Value	Unit
Γ_d	Interfacial debonding energy	0.1	J/m^2
τ	Interfacial shear stress	18	MPa
Γ_{m0}	Fracture energy at the first matrix cracking	6[3]	J/m^2
$\Gamma_{m_{max}}$	Maximum fracture energy	37.1	J/m^2
ρ_0	Characteristic matrix crack density	4.38	mm^{-1}
a	Coefficient related to the variation of defects	0.763	—
σ_c	Characteristic fiber strength	2.25[18]	GPa
m_f	Weibull shape parameter related to fiber strength	1.7[18]	—
f_d	Number of defects for initial damage per characteristic length δ_c	0	—
P_p	Probability of crack propagation from the matrix to the fibers	0.06	—

regarded as the probability P_p that matrix cracks propagate into the fibers. Accordingly, the probability was obtained as follows.

$$P_p = 1 - F\left(\sigma^*_{deb}\right) = 0.06 \quad \cdots\cdots\cdots\cdots\cdots\cdots \quad (4\text{-}14)$$

The parameters related to the LLS model are described in detail by Haruyama et al.[22]

4.3 Calculation results

Figure 11 shows the comparison between the calculated and experimental stress–strain relationships. These results show that the calculated tangent modulus after matrix crack saturation agreed well with the experimental results. Although the GLS model overestimated the fracture strain, the results were improved by the LLS model. In addition, although the LLS model underestimated the value, it approximately predicted the experimental fracture strength.

5. Conclusion

Matrix crack growth calculations considering the variation of defects were performed using the energy-based matrix crack growth model in combination with the Monte Carlo method. As a result, the calculated stress–strain relationship agreed well with the experimental results up to the initial pseudo-ductile region, while the calculated crack density–stress relationship also agreed well with the experimental results throughout the entire process from crack initiation to saturation. Furthermore, a periodic matrix crack growth model was investigated, and it was shown that results equivalent to those of the random matrix crack growth calculations using the Monte Carlo method could be obtained by introducing a correction coefficient. Furthermore, the GLS and LLS models, which consider the probability of matrix crack propagation into the fibers, were used as fiber breakage models. As a result, the LLS model accurately predicted the experimental fracture strain and, although it underestimated the value, also approximately predicted the experimental fracture strength.

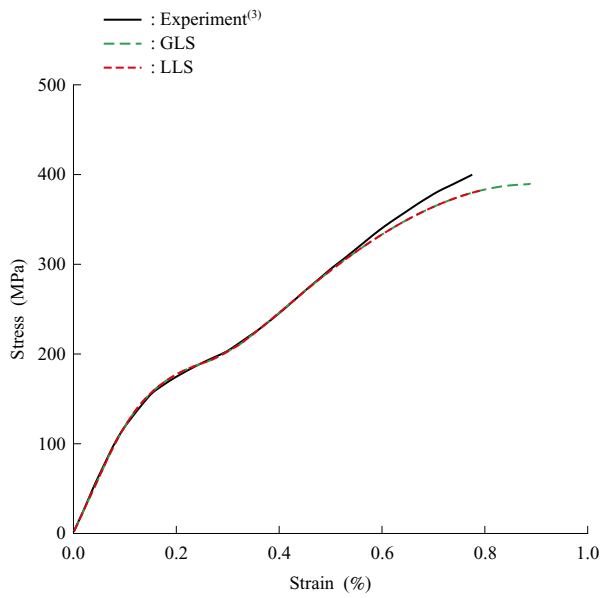


Fig. 11 Stress–strain curves for experimental, GLS and LLS results

The static tensile model for unidirectional CMCs described in this paper has also been extended to cross-ply CMCs. The model and the verification method are described in detail by Haruyama et al.[15], [22]

— Acknowledgments —

We would like to acknowledge the support of Professor Tomonaga Okabe, Department of Aerospace Engineering, Tohoku University, and Associate Professor Yoshiaki Kawagoe, Research Center for Green X-Tech, Tohoku University. We express our sincere gratitude to them.

REFERENCES

(1) D. Haruyama, Y. Kawagoe and T. Okabe : Analytical modeling of energy-based matrix crack growth and fiber breakage in unidirectional ceramic matrix composites under static tensile behavior in the longitudinal direction, Advanced Composite Materials, 2024

(2) F. W. Zok and S. M. Spearing : Matrix crack spacing in brittle matrix composites, Acta Metallurgica et Materialia, Vol. 40, No. 8, 1992, pp. 2033-2043

(3) A. W. Pryce and P. A. Smith : Behaviour of unidirectional and crossply ceramic matrix composites under quasi-static tensile loading, Journal of Materials Science, Vol. 27, 1992, pp. 2695-2704

(4) M. J. Blissett, P. A. Smith and J. A. Yeomans : Thermal shock behaviour of unidirectional silicon carbide fibre reinforced calcium aluminosilicate, Journal of Materials Science, Vol. 32, 1997, pp. 317-325

(5) T. J. Mackin and F. W. Zok : Fiber Bundle Pushout: A Technique for the Measurement of Interfacial Sliding Properties, Journal of the American Ceramic Society, Vol. 75, No. 11, 1992, pp. 3169-3171

(6) J.-M. Domergue, E. Vagaggini and A. G. Evans : Relationships between Hysteresis Measurements and the Constituent Properties of Ceramic Matrix Composites: II, Experimental Studies on Unidirectional Materials, Journal of the American Ceramic Society, Vol. 78, No. 10, 1995, pp. 2721-2731

(7) M. He, B.-X. Wu, A. G. Evans and J. Hutchinson : Inelastic strains due to matrix cracking in unidirectional fiber-reinforced composites, Mechanics of Materials, Vol. 18, No. 3, 1994, pp. 213-229

(8) E. Vagaggini, J.-M. Domergue and A. G. Evans : Relationships between Hysteresis Measurements and the Constituent Properties of Ceramic Matrix Composites: I, Theory, Journal of the American Ceramic Society, Vol. 78, No. 10, 1995, pp. 2709-2720

(9) D. S. Beyerle, S. M. Spearing, F. W. Zok and A. G. Evans : Damage and Failure in Unidirectional Ceramic-Matrix Composites, Journal of the American Ceramic Society, Vol. 75, No. 10, 1992, pp. 2719-2725

(10) D. Marshall : Analysis of fiber debonding and sliding experiments in brittle matrix composites, Acta Metallurgica et Materialia, Vol. 40, No. 3, 1992, pp. 427-441

(11) J. Sánchez, M. Elizalde, A. Daniel, J. Martinez-Esnaola,

I. Puente and A. Martin : Interfacial characterization of 2D woven SiC/SiC and cross-ply 0°/90° CAS/SiC composites, Composites Part A: Applied Science and Manufacturing, Vol. 27, No. 9, 1996, pp. 787-792
(12) A. G. Evans, J.-M. Domergue and E. Vagaggini : Methodology for Relating the Tensile Constitutive Behavior of Ceramic-Matrix Composites to Constituent Properties, Journal of the American Ceramic Society, Vol. 77, No. 6, 1994, pp. 1425-1435
(13) A. Rényi : On a One-Dimensional Problem Concerning Random Space-Filling, Publication of the Mathematical Institute of the Hungarian Academy of Sciences, Vol. 3, 1958, pp. 109-127
(14) A. Kimber and J. Keer : On the theoretical average crack spacing in brittle matrix composites containing continuous aligned fibres, Journal of Materials Science Letters, Vol. 1, No. 8, 1982, pp. 353-354
(15) D. Haruyama, Y. Kawagoe and T. Okabe : Analytical modeling of matrix and transverse crack growth and fiber breakage for predicting the static tensile behavior of cross-ply ceramic matrix composites, Materials System, Vol. 42, 2025, pp. 3-20
(16) S. L. Phoenix and R. Raj : Overview no. 100 Scalings in fracture probabilities for a brittle matrix fiber composite, Acta Metallurgica et Materialia, Vol. 40, No. 11, 1992, pp. 2813-2828
(17) H. E. Daniels : The Maximum of a Gaussian Process Whose Mean Path Has a Maximum, with an Application to the Strength of Bundles of Fibres, Advances in Applied Probability, Vol. 21, No. 2, 1989, pp. 315-333
(18) W. A. Curtin : Stochastic damage evolution and failure in fiber-reinforced composites, Advances in Applied Mechanics, Vol. 36, 1998, pp. 163-253
(19) M. Y. He, A. G. Evans and J. W. Hutchinson : Crack deflection at an interface between dissimilar elastic materials: Role of residual stresses, International Journal of Solids and Structures, Vol. 31, No. 24, 1994, pp. 3443-3455
(20) L. L. Snead, D. Steiner and S. J. Zinkle : Interfacial push-out measurements of fully-bonded SiC/SiC composites, Conference: Symposium on composites, 1990
(21) M. D. Thouless, O. Sbaizero, L. S. Sigl and A. G. Evans : Effect of interface mechanical properties on pullout in a SiC-fiber-reinforced lithium aluminum silicate glass-ceramic, Journal of the American Ceramic Society, Vol. 72, No. 4, 1989, pp. 525-532
(22) D. Haruyama, Y. Kawagoe and T. Okabe : Monte Carlo simulation with energy-based matrix and transverse crack growth model for cross-ply ceramic matrix composites under static tensile behavior, Advanced Composite Materials, 2025